

RESEARCH

Open Access



Flexural Behavior of Circular Hollow RC Piers with Reduced Amounts of Inner Hoops

Zhong-Xian Li¹, Chun-yu Du¹, Xiao Liang^{2*} and Bo Zhao¹

Abstract

Reversed cyclic loading tests of two circular hollow RC piers were conducted in this study to investigate the effect of different amounts of inner and outer circular hoops on their flexural behavior. The test results showed that the column with a smaller amount of inner circular hoops presented better flexural response than the as-built column with an equal amount of inner and outer circular hoops. Also, the demand developed on the inner circular hoops was smaller than the outer one within the plastic hinge regions, which verified that using a smaller amount of inner circular hoops was reasonable and effective. By examining the confining stress experienced by the concrete in the radial and circumferential directions based on a detailed theoretical analysis, a modeling approach was proposed to take the confinement effect in circular hollow RC piers into consideration. The proposed modeling approach was validated through comparisons with the experimental study and satisfactory agreement was found.

Keywords: circular hollow piers, confinement, flexural behavior, modeling, testing

1 Introduction

Long-span and high-elevation concrete bridges have been constructed throughout the world, such as *Mil-lau Viaduct* in France, *San Marcos Bridge* in Mexico, *Hezhang Bridge* in China. Incorporating hollow sections to bridge piers for long-span and high-elevation concrete bridges have gained popularity due to their improved structural efficiency compared to solid concrete piers.

It is well known that the rotation of plastic hinges usually provides the ductility of bridge piers, and the rotation capacity of plastic hinges relies on the development of inelastic strains of reinforcement and concrete within the plastic hinge regions (Priestley et al. 1996). One of the key factors that help to increase the strength and ductility of a bridge pier is the confining effect provided by the transverse reinforcement (Penelis and Kappos 1997; Pinto et al. 2003; Hwang and Yun 2004; Calvi et al. 2005). The overall response of solid and hollow rectangular

piers under lateral loads has been shown to be improved by detailing the transverse reinforcement configurations. An experimental study on confinement effectiveness of cross-ties in RC rectangular columns was conducted by Moehle and Bavanagh (1985). They found that cross-ties having 180° hooks were as effective in confining concrete as intermediate hoops. Han et al. (2013), Prado et al. (2016) and Liao et al. (2017) discussed the effect of different transverse reinforcement configurations on the flexural behavior of solid or hollow rectangular columns, such as lateral displacement capacity and failure mode. Furthermore, there has been additional research on detailing transverse reinforcement to improve the ductility of circular hollow columns. Circular hollow concrete piers have been designed with two layers of an equal amount of both longitudinal and transverse reinforcement that are uniformly placed near both the inside and outside concrete wall surfaces. These two layers of transverse reinforcement are connected with cross-ties, which usually have the same bar size as the transverse reinforcement for simplicity (Yeh et al. 2001, 2002; Mo et al. 2003). The amount and spacing of transverse reinforcement in hollow piers have been designed based on the requirements of solid piers without fully understanding of

*Correspondence: xliang@tcu.edu.cn

²Tianjin Key Laboratory of Civil Structure Protection and Reinforcement, Tianjin Chengjian University, Tianjin 300384, China
Full list of author information is available at the end of the article
Journal information: ISSN 1976-0485 / eISSN 2234-1315

confinement effect in hollow piers. Besides, limited information was available for the requirements of cross-ties detailing and the rationale of placing an equal amount of the inner and outer transverse reinforcement in hollow concrete piers was not provided, nor were measurements taken to support this design assumption (Liang and Sritharan 2018).

Yeh et al. (2001) investigated the effects of ductility and dissipated energy of three hollow circular bridge piers. Based on their finite element analysis, the inside transverse reinforcement was not required due to confining not existing pressure. Papanikolaou and Kappos (2009a, b) performed a parametric analysis on approximately 180 piers (circular, square, solid, and hollow sections) that were subjected to axial compression, using three-dimensional finite element analysis. They found that the inner and outer transverse reinforcement are required to be connected with cross-ties to provide satisfactory confining effect. If the inner transverse reinforcement was not connected to the outer transverse reinforcement through cross-ties effectively, the inner transverse reinforcement only confined the inside concrete cover, causing the concrete region located outside this inner transverse reinforcement to be negatively confined. However, the experimental study conducted by Lee et al. (2015) showed that two identical columns, one with cross-ties and the other one without cross-ties, did not show a significant difference between their responses, which contradicted with the analytical results found by Papanikolaou and Kappos (2009a, b). It was shown that the strain of cross-ties measured at the column height of 200 mm was higher than about 67% of the yield strain. Based on the observations, the conclusion is that the cross-ties did not improve the column ductility but helped to delay the buckling of longitudinal reinforcing bars for compression-controlled sections. Also, the study showed that a large amount of outer transverse reinforcement helped to decrease the damaged area of the inside concrete wall face and the inside transverse reinforcement amount did not influence the behavior of hollow piers in the case of both flexure-controlled and compression-controlled sections.

Currently, many studies quantified the confining effect and established the stress–strain relation in hollow piers confined with FRP (such as Rousakis et al. 2007; Cascard et al. 2016), but limited effort had been made towards hollow piers with regular transverse reinforcement. A recent study by Liang and Sritharan (2018) quantified the confined concrete strength of hollow piers with different confinement reinforcement configurations using 3D nonlinear finite element method. The modeled hollow piers were subjected to axial compression. It was found that the confined concrete strength of circular hollow

piers increased by 15% as the inner-to-outer transverse reinforcement ratio varied from 5:5 to 1:9. This is because the demand developed on the inner circular hoops was transferred to the outer circular hoops through cross-ties. Therefore, they concluded that the required amounts of inner circular hoops should be much smaller than the outer circular hoops, when the wall thickness ratio is in the range of 0.125 to 0.2. This finding was consistent with the conclusions drawn by Lee et al. (2015), but was different from what has been suggested in the literature and used in practice.

To investigate the effect of different amounts of the inner and outer circular hoops on the flexural performance of circular hollow concrete piers and determine the confining stress in these piers, two large-scale circular hollow concrete piers were tested under a combination of constant axial load and cyclic reversed lateral load, as described below. After that, an analytical approach was proposed and validated to account for the confining effect of transverse reinforcement in circular hollow RC piers.

2 Experimental Study

2.1 Test Columns

In this study, two circular hollow RC columns with the same section dimensions, the same longitudinal reinforcement ratio, the same volumetric ratio of transverse reinforcement, but different amounts of the inner and outer circular hoops, called herein S3 and S4, were constructed. The section properties of both columns are illustrated in Fig. 1 and summarized in Table 1. The columns that capture the characteristics of existing hollow columns were designed based on the current seismic design code (Caltrans Seismic Design Criteria 2017; JTG/T B02-01—2008 2008). The outer diameter of both columns was 1000 mm and the inner diameter was 600 mm, which led to a wall thickness of 200 mm or a wall thickness ratio of 0.2. The circular hollow bridge columns in practice are typically 3–6 m in diameter and with longitudinal reinforcing bars of D36 (i.e., $d_b = 36$ mm) or larger, thus, the scale was targeted to be 1:5 in this program. The distance between the lateral loading point and the top surface of the base block was 3850 mm, tested in single bending to give an aspect ratio of 3.85.

Eighteen longitudinal reinforcing bars with a diameter of 18 mm were distributed evenly near the outside and inside concrete wall surfaces, respectively. The resulting longitudinal reinforcement ratio to the gross section (i.e., ignoring the void in the hollow section) was 1.17% for both columns.

The amount and spacing of transverse reinforcement are essential for the seismic design of bridge columns. In this test program, both columns were reinforced with

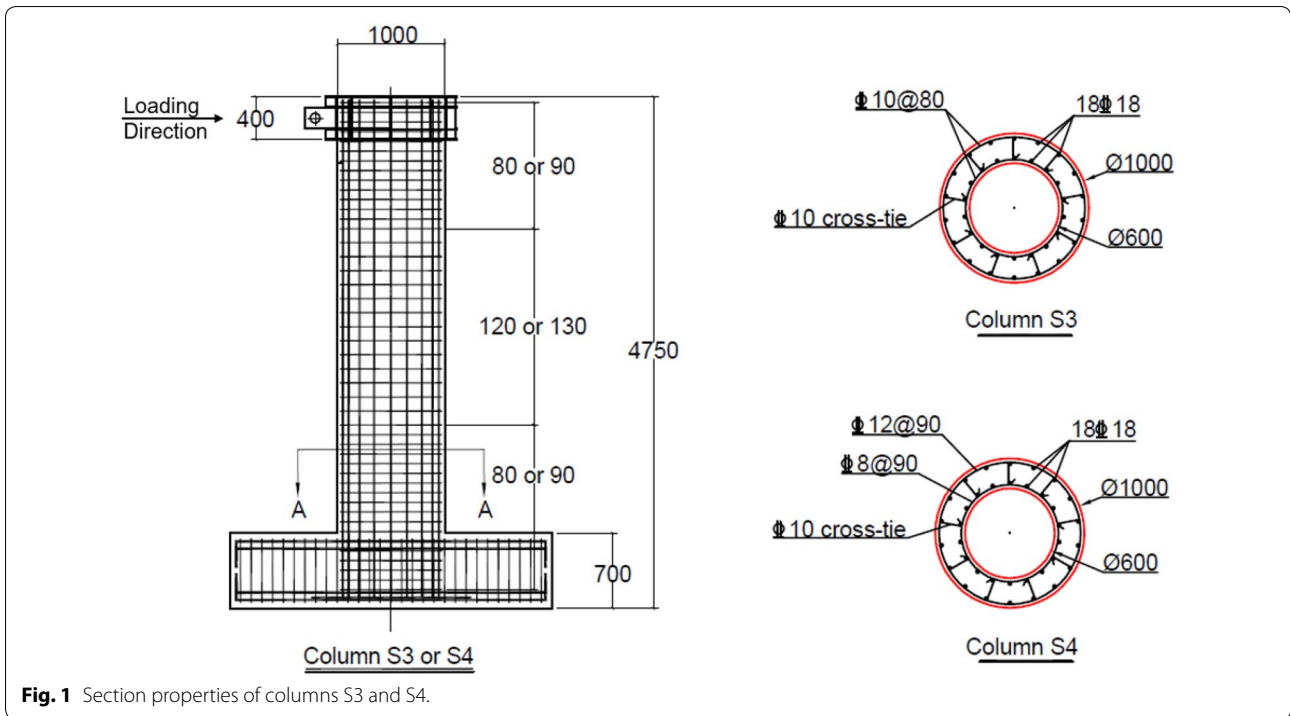


Fig. 1 Section properties of columns S3 and S4.

Table 1 Test columns details.

| Column | Inner-to-outer reinforcement ratio | Longitudinal reinforcement | | | | Transverse reinforcement | | | | Axial load ratio |
|--------|------------------------------------|----------------------------|-------|--------------|------|--------------------------|-------|--------------|------|------------------|
| | | Num. & d_l (mm) | | ρ_l (%) | | d_t (mm) | | ρ_s (%) | | |
| | | Outer | Inner | Gross | Net | Outer | Inner | Gross | Net | |
| S3 | 5:5 | 18–18 | 18–18 | 1.17 | 1.82 | 10 | 10 | 0.63 | 0.98 | 0.06 |
| S4 | 4:9 | 18–18 | 18–18 | 1.17 | 1.82 | 12 | 8 | 0.63 | 0.97 | |

two layers of circular hoops connected with cross-ties. An equal amount of the inner and outer circular hoops was provided for column S3, with the diameter being 10 mm for both the inner and outer circular hoops. The spacing of circular hoops was 80 mm within the plastic end region and column top region, and 120 mm in other regions. For column S4, the diameters of transverse reinforcement were 12 mm for the outer circular hoops and 8 mm for the inner circular hoops. The spacing was 90 mm within the plastic end region and column top region, and 130 mm in other regions, to maintain the same volumetric ratio of transverse reinforcement as column S3. The resulting inner-to-outer transverse reinforcement amount ratio was 5:5 and 4:9 for columns S3 and S4, respectively. The volumetric ratio of transverse reinforcement for both columns was 0.63% based on the gross section, which meet the displacement ductility performance requirements through inelastic pushover analysis using the nonlinear finite

element analysis program OpenSees (i.e., Open System for Earthquake Engineering Simulation). Also, the selected longitudinal spacing was satisfied for anti-buckling requirement of the transverse reinforcement expressed by Eq. (1). However, the provided number of cross-ties was significantly smaller than those required by JTG/T B02-01–2008 (2008) to simplify the construction process, as shown in Fig. 1.

$$s_{\max} = \min \left\{ \frac{1}{5}b, 6d_l, 203 \text{ mm} \right\} \quad (1)$$

2.2 Material Properties

The measured yield and ultimate strengths of transverse and longitudinal reinforcing bars are listed in Table 2. The measured concrete compressive strength of columns S3 and S4 on the day of testing was 33.8 MPa and 31.6 MPa, respectively.

Table 2 Material properties of reinforcement.

| Reinforcement diameter (mm) | Young's modulus (MPa) | Yield strength (MPa) | Ultimate strength (MPa) |
|-----------------------------|-----------------------|----------------------|-------------------------|
| 18 | 2.08×10^5 | 457 | 612 |
| 12 | | 496 | 563 |
| 10 | | 476 | 663 |
| 8 | | 493 | 666 |

2.3 Test Setup and Loading Sequence

Figure 2 shows the test setup. The tests were conducted in the Key Laboratory of Coast Civil Structure Safety of the Education Ministry of Tianjin University, China. As shown in Fig. 2, the reversed cyclic lateral load was applied by the horizontal hydraulic actuator, which has a loading capacity of 2000 kN with a maximum displacement of ± 500 mm. A total vertical load of 1600 kN was applied and maintained throughout the test, corresponding to an axial load ratio of 6% based on the gross section and 9.4% based on the net section.

A total of 54 strain gauges were mounted on the outer longitudinal reinforcing bars and outer circular hoops. Additional 24 strain gauges were placed on the inner

longitudinal reinforcing bars, inner circular hoops, and cross-ties within the potential plastic hinge region, to monitor the strains of columns S3 and S4 during the test. The gauge layout is shown in Fig. 3, in which 1–10 represents the location for the longitudinal reinforcing bars, while N, S, E, W, NW, SW, NE, and SE represents the location for the transverse reinforcing bars and cross-ties.

Six vertical Linear Variable Displacement Transducers (LVDTs) were mounted each on the east and west faces for the section curvature measurement over the plastic hinge region. A string LVDT was applied to measure the lateral displacement at the loading point (see Fig. 2).

The lateral load was applied under force–displacement control in a pseudo-static matter. The test sequence consisted of single cycles at 25%, 50%, 75% and 100% of the theoretical yield force, which was calculated based on a moment–curvature analysis of column sections using the nonlinear finite element analysis program OpenSees. After the outer tensile longitudinal reinforcing bars yielded, that is the strain measured by strain gauges attached to the longitudinal reinforcing bar located right above the column–footing interface reached $2200 \mu\epsilon$, the lateral load was switched to displacement control by increasing ductility levels in a sequence of 1.0, 1.5, 2.5,

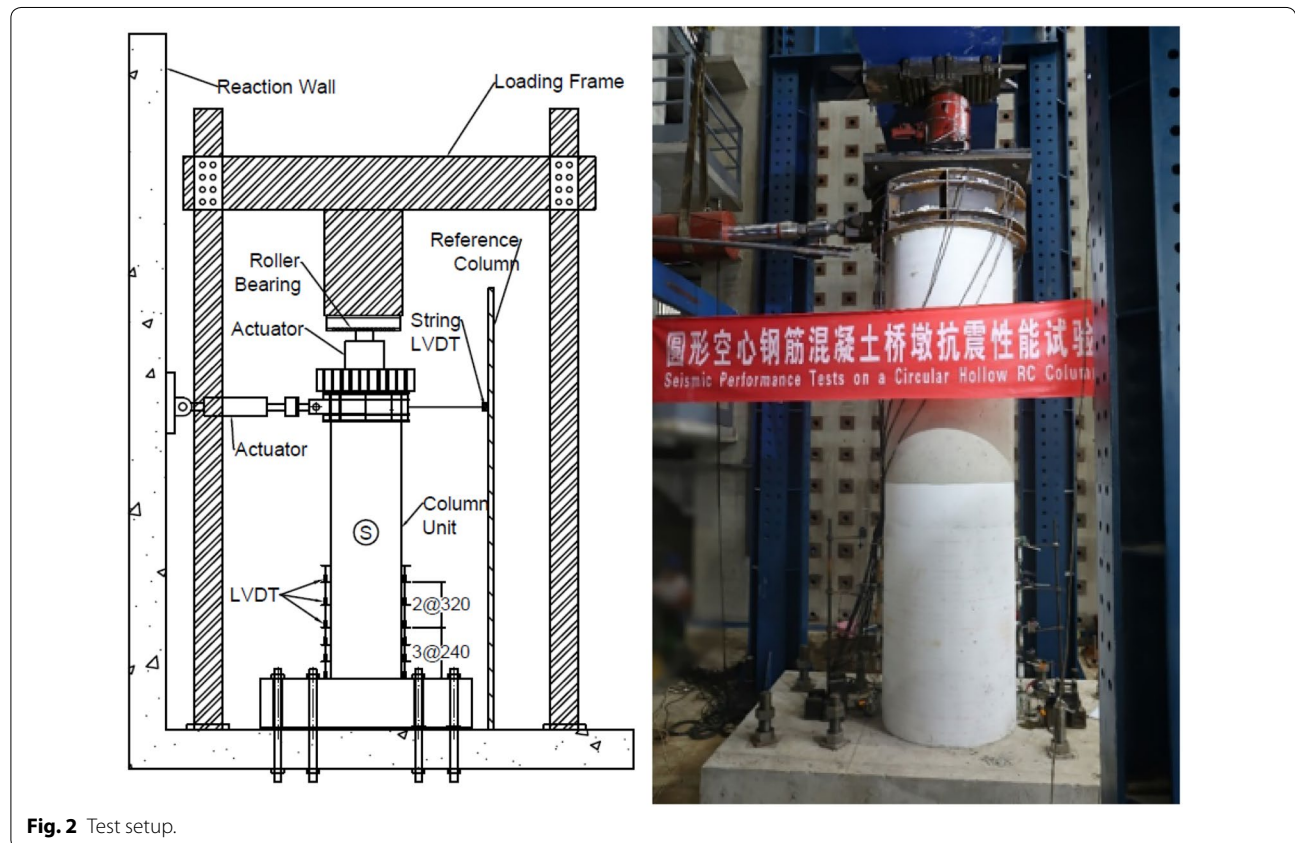
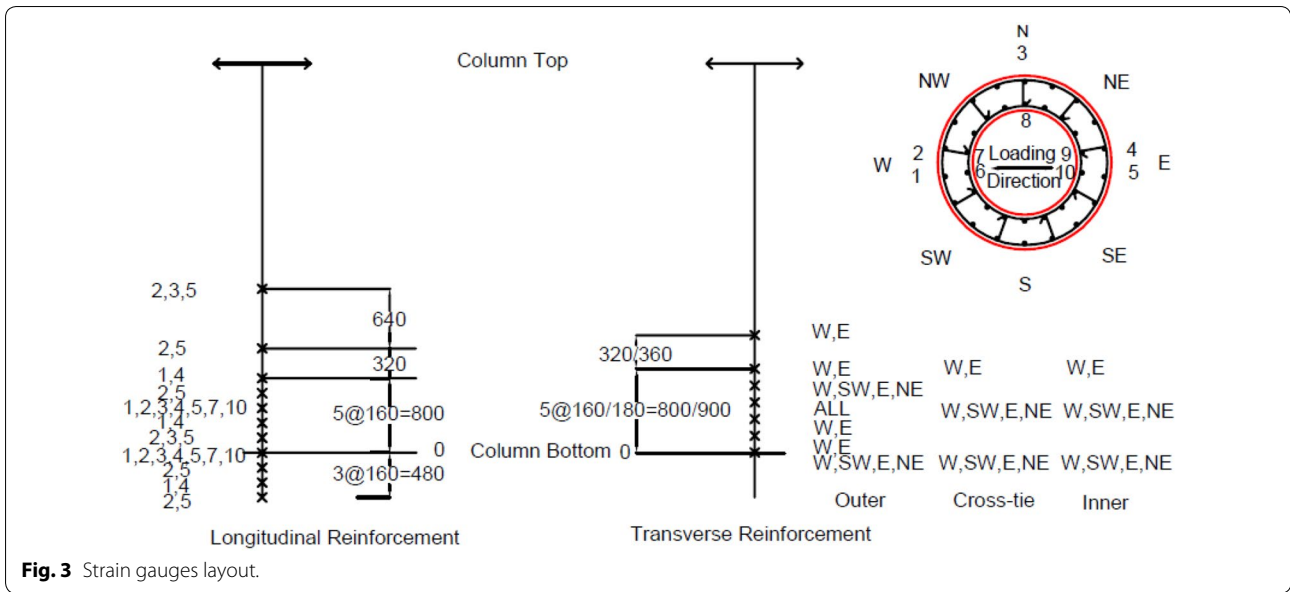


Fig. 2 Test setup.



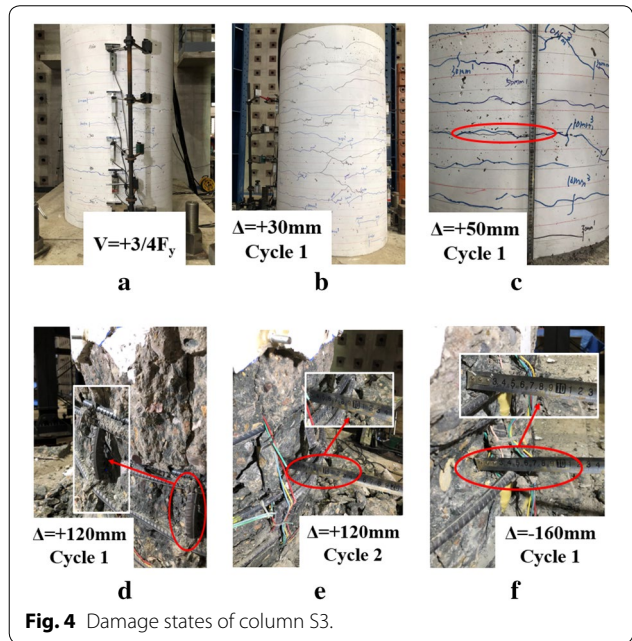
3.5, 4.5,..., respectively, until the failure occurred. Three cycles at each target displacement ductility level were repeated.

3 Experimental Results and Discussion

3.1 General Observations

The lateral load was applied along the west–east direction. The failure modes of both columns were flexure failure. After the longitudinal reinforcing bars experienced yielding, the column S4 was able to develop a more stable response under cycles of load reversals compared to the column S3. The failure of column S3 was characterized by significant concrete spalling, followed by longitudinal reinforcing bars buckling. The failure of column S4 was characterized by the fracture of longitudinal reinforcing bars when the displacement was 145 mm. The general observations for each column are described as follows:

Column S3 The first series of flexural cracks occurred with a well-distributed spacing of approximately 200 mm when the lateral load reached $3/4F_y$, as shown in Fig. 4a. Then, the outer tensile longitudinal reinforcing bar yielded and the average yield displacement measured at the horizontal loading point was about 20 mm, corresponding to a ductility of 1. After the longitudinal reinforcing bars yielded and up to the first push cycle to a displacement of 30 mm (i.e., ductility=1.5), many new flexural cracks appeared and the spacing decreased to approximately 100 mm. Also, existing cracks extended and became inclined on the north and south sides, as shown in Fig. 4b. During the first cycle to a displacement of 50 mm (i.e., ductility=2.5), flexural cracks widened significantly at the column height of 350 mm and



250 mm from the base on the west and east side, respectively, as shown in Fig. 4c. During the first cycle to a displacement of 70 mm (i.e., ductility=3.5), cover concrete started crushing on the east side from the column height of 200 mm to 500 mm, and experienced serious spalling during the second cycle to displacement of 70 mm. However, cover concrete did not experience any significant crushing on the west side until the displacement reached 90 mm (i.e., ductility=4.5). Finally, confined concrete crushed, and three longitudinal reinforcing bars buckled

in the compression region at column base during the first push cycle to a displacement of 120 mm (i.e., ductility=6) as shown in Fig. 4d. Concrete wall lost more than 50% wall thickness (i.e., 100 mm), as shown in Fig. 4e and additional one longitudinal reinforcing bars buckled, along with more than 40% reduction of peak load in the second push cycle to a displacement of 120 mm. Therefore, the test was terminated in the push direction and continued in the pull direction until the displacement reached 160 mm (i.e., ductility=8), when more than 50% wall thickness (i.e., 100 mm) was lost on the west side, as shown in Fig. 4f.

Column S4 During the cycle to $3/4F_y$, a series of flexural cracks appeared with a well-distributed spacing of approximately of 200 mm, as shown in Fig. 5a. As the load increased, many new flexural cracks occurred on both the west and east sides of the column with a reduced spacing of approximately 100 mm and the outer longitudinal reinforcing bar yielded. The average yield displacement of column S4 measured at the horizontal loading point was about 17 mm, corresponding to a ductility of 1. Subsequently, additional flexural cracks formed and extended to the north and south sides, and many shear cracks appeared on the north and south sides. During the second push cycle to a displacement of 40 mm (i.e., ductility=2.5), flexural cracks widened significantly at the column height of 200 to 450 mm from the base on the west side, as shown in Fig. 5b. The cover concrete started crushing in the first push cycle to a displacement of 55 mm (i.e., ductility=3.5) and 75 mm (i.e., ductility=4.5) on the east and west side, respectively,

as shown in Fig. 5c. Crack width continued to increase, and a significant amount of concrete spalled off when the displacement reached 95 mm (i.e., ductility=5.5). After that, confined concrete crushed, and one longitudinal reinforcing bars buckled in the compression region at column base on the west side during the first push cycle to a displacement of 120 mm (i.e., ductility=7). During the second push cycle to a displacement of 120 mm, three longitudinal reinforcing bars buckled on the east side and two longitudinal reinforcing bars buckled on the west side. Concrete spalled off up to a height of 450 mm on the east side and 250 mm on the west side, as shown in Fig. 5d. During the third pull cycle to a displacement of 120 mm, confined concrete experienced serious crushing and buckling of longitudinal reinforcing bars was obvious. Finally, during the first push cycle to a displacement of 145 mm (i.e., ductility=8.5), concrete wall lost 40 mm thickness on both the east and west sides. The core concrete continued to spall off, and concrete wall lost 60 mm thickness on the west side during the first pull cycle to a displacement of 145 mm. During the second cycle to a displacement 145 mm, four longitudinal reinforcing bars buckled, concrete wall lost 70 mm thickness, as shown in Fig. 5e, and two longitudinal reinforcing bars ruptured, as shown in Fig. 5f.

3.2 Hysteretic Response

The measured lateral force–displacement hysteretic responses of columns S3 and S4 are plotted in Fig. 6. As shown in Fig. 6, both columns exhibit a rounded shape, which shows good energy dissipation and hysteretic performance. At the initial loading stage, both columns were in the elastic stage. The residual deformation was very small, and the stiffness degradation was not noticeable. More than 30% reduction of the initial secant stiffness was observed for both columns at $V=3/4F_y$, due to the appearance of horizontal cracks on the west and east surfaces. After the outer tensile longitudinal reinforcing bars yielded, the columns entered the plastic deformation stage and a considerable stiffness degradation of both columns was observed at the ductility 3.5, when cover concrete spalled seriously on the east surface. Compared with the initial loading stage, the secant stiffness at the ductility of 3.5 was decreased by 74.5% and 68.9% for columns S3 and S4, respectively. Additionally, compared to column S3, the column S4 showed a more stable response under cycles of load reversals with a lower amount of confined concrete crushing (70 mm vs. 100 mm concrete wall thickness lost) at the ultimate ductility. This observation reflected better confinement effectiveness of a 4:9 inner-to-outer transverse reinforcement amount ratio since confinement of concrete by transverse

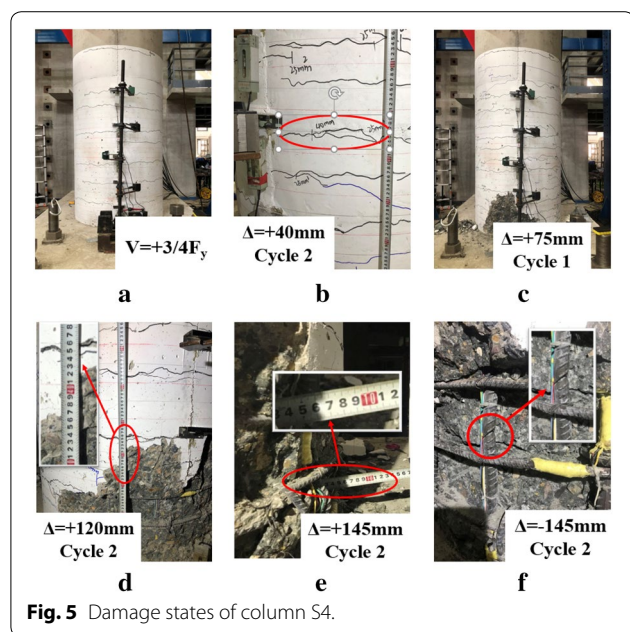
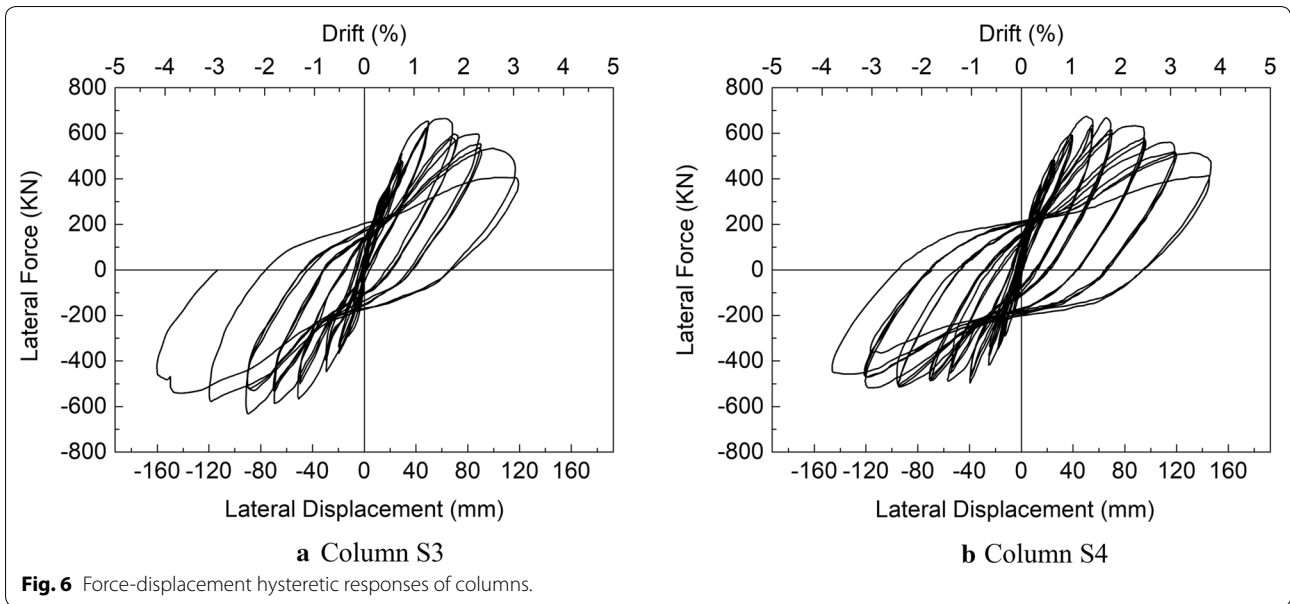


Fig. 5 Damage states of column S4.

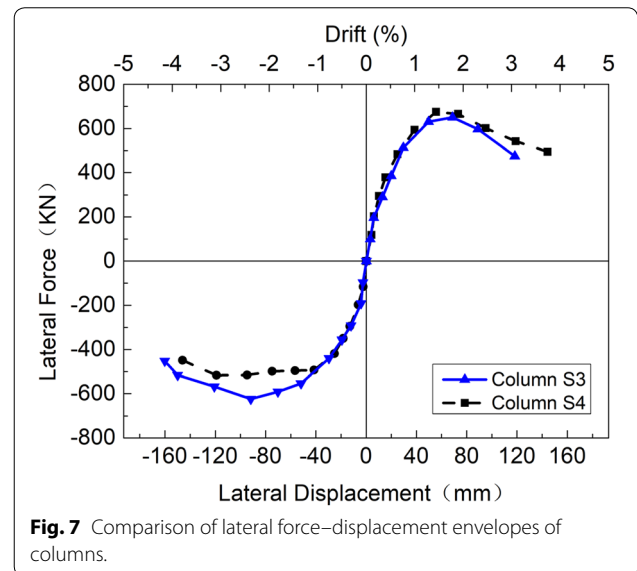


reinforcement increases both the compressive strain and stress of confined concrete.

3.3 Ductility Factors

Figure 7 shows the determined envelopes of lateral force–displacement hysteretic response. Displacement ductility is a parameter that reflects the ductile response of structural components, and it can be found as the ratio of the displacement at ultimate to that at yield (i.e., $\mu_{\Delta} = \Delta_u / \Delta_y$). Here, the yield displacement Δ_y was defined as the lateral displacement measured at the horizontal loading point when the outer tensile longitudinal reinforcing bar yielded, and the ultimate displacement Δ_u was obtained when the outer tensile longitudinal reinforcing bars fractured, or the load bearing capacity of column dropped to 80% of peak value, whichever occurred first. These values are given in Table 3.

As Fig. 7 shows, the load bearing capacity reaches the peak value at the ductility of 3.5 for columns S3 and S4 in the push direction. Because two layers of transverse reinforcement provides a satisfactory confinement effect to core concrete, the load bearing capacity was maintained above 80% of the peak value over the next two loading levels. Comparing the column S3 with column S4, the load bearing capacity of column S4 decreased more slowly. For example, when the lateral displacement was 120 mm in the push direction, the load bearing capacity of columns S3 and S4 dropped to 73% and 80% of the peak value, respectively. Additionally, the displacement ductility for columns S3 and S4 are 6.7 and 7.8,



respectively. Compared to column S3, the displacement ductility of column S4 was increased by 16.4% at a given volumetric transverse reinforcement ratio of 0.63% based on the gross section. Importantly, this increase was primarily due to the increase of displacement capacity of the column S4 that was attributed mainly to the better confinement effect provided by a 4:9 inner-to-outer transverse reinforcement amount ratio. This is because both columns had identical dimensions and reinforcing reinforcement details, only the inner-to-outer layer of transverse reinforcement amount ratio was different.

Table 3 Force-displacement responses of columns S3 and S4.

| Column | Yield displacement (mm) | | | Ultimate displacement (mm) | | | Peak load (kN) | | | Displacement ductility (μ_{Δ}) | | |
|--------|-------------------------|----------|------|----------------------------|----------|-------|----------------|----------|-------|---|----------|------|
| | Push (+) | Pull (-) | Avg. | Push (+) | Pull (-) | Avg. | Push (+) | Pull (-) | Avg. | Push (+) | Pull (-) | Avg. |
| S3 | 22 | 18 | 20 | 110 | 152 | 131 | 650 | 625 | 637.5 | 5.0 | 8.4 | 6.7 |
| S4 | 16 | 18 | 17 | 120 | 145 | 132.5 | 675 | 520 | 597.5 | 7.5 | 8.1 | 7.8 |

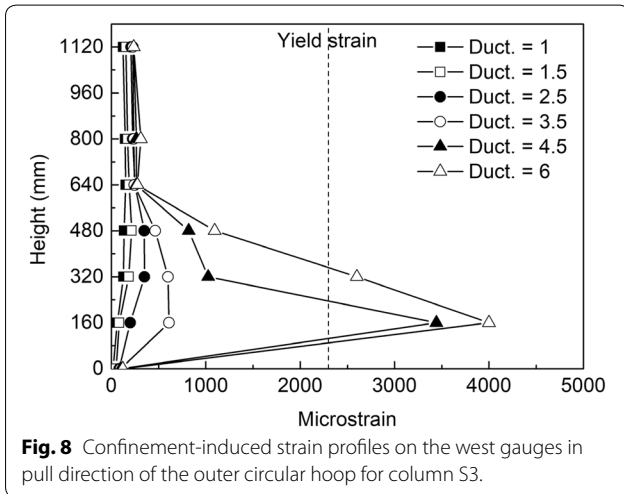


Fig. 8 Confinement-induced strain profiles on the west gauges in pull direction of the outer circular hoop for column S3.

3.4 Confinement-Induced Transverse Strain within the Plastic Hinge Region

Since the lateral force was applied in the east–west direction, the east or west face is in compression at the column base, and the transverse reinforcement provides confinement. Therefore, the strains measured on east gauges in the push direction and west gauges in the pull direction were examined for confinement effect.

3.4.1 Outer Circular Hoop

The maximum confinement-induced strain profiles of the outer circular hoops for column S3 at different column heights for each ductility level are plotted in Fig. 8. From this figure, significant confinement-induced strains increase as the ductility increase from 3.5 to 4.5, when the onset of concrete crushing was noted. In addition, the strains measured at the column height of 160 mm, 320 mm, and 480 mm increased significantly with each increasing of ductility level as compared with those in other heights, indicating that the inelastic deformation was primarily concentrated over the column height of 480 mm from the base. Similar confinement-induced strain profiles of the outer circular hoops within the plastic hinge region was obtained for column S4. The first major increase in confinement-induced strains of

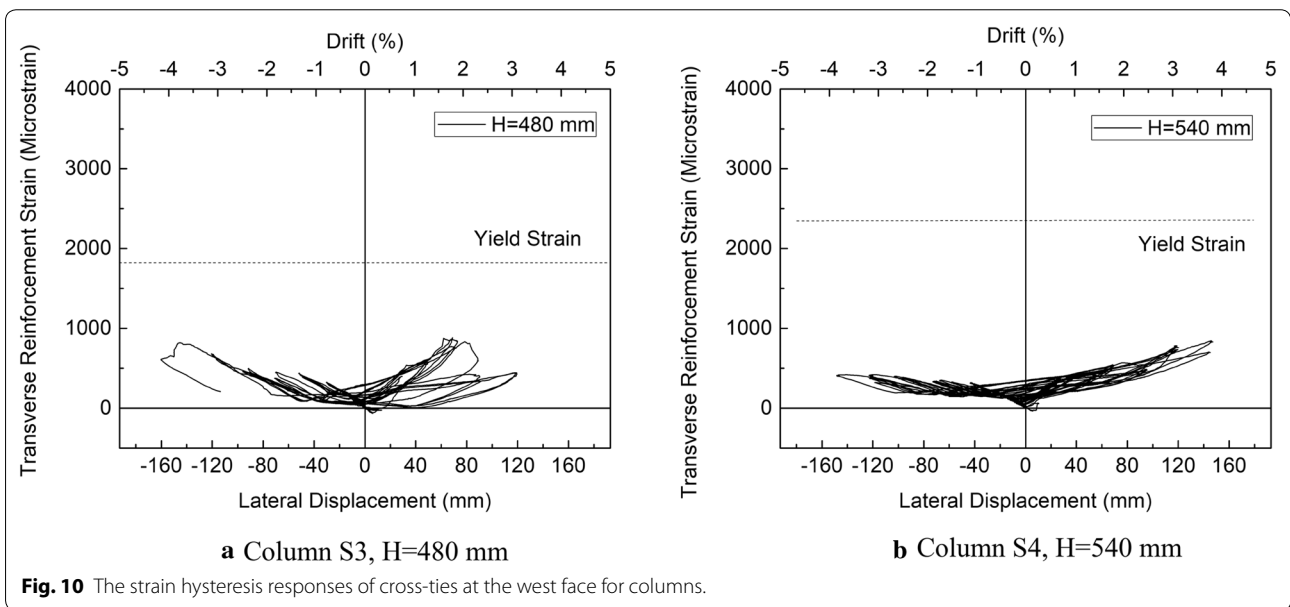
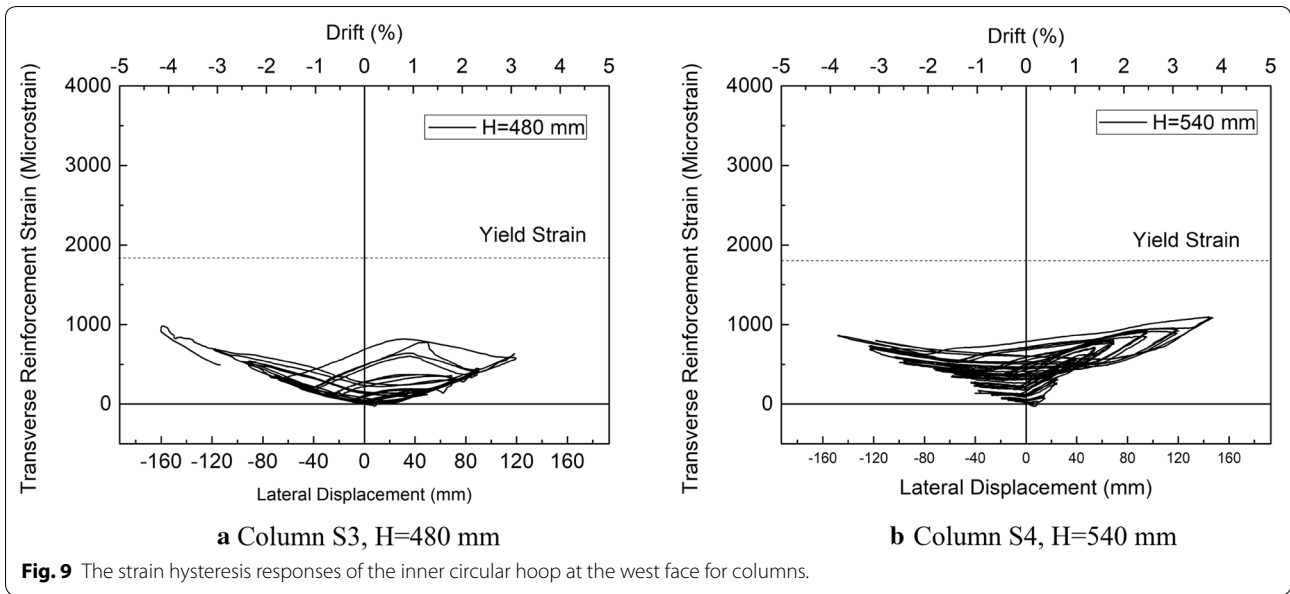
the outer circular hoop for column S4 was observed as the ductility increased from 2.5 to 3.5 when concrete started to experience crushing. The theoretical plastic hinge length proposed by Priestley et al. (1996) is 490 mm, which provides a reasonable estimation for circular hollow piers with two layers of circular hoops and cross-ties.

3.4.2 Inner Circular Hoop and Cross-ties

Figures 9 and 10 show the confinement-induced strain hysteresis responses of the inner circular hoops and cross-ties at the column height of 480 and 540 mm for columns S3 and S4, respectively. Based on these figures, the confinement-induced strains of the inner circular hoops and cross-ties increase with each increase of ductility level. However, the maximum induced strains of inner circular hoops and cross-ties at the ultimate ductility level are below the yield strain. This is because strain gauges were not placed on the inner circular hoops and cross-ties between the column heights of 0 to 480 mm, where the maximum curvature would be expected.

3.4.3 Effect of Inner-to-Outer Transverse Reinforcement Ratio

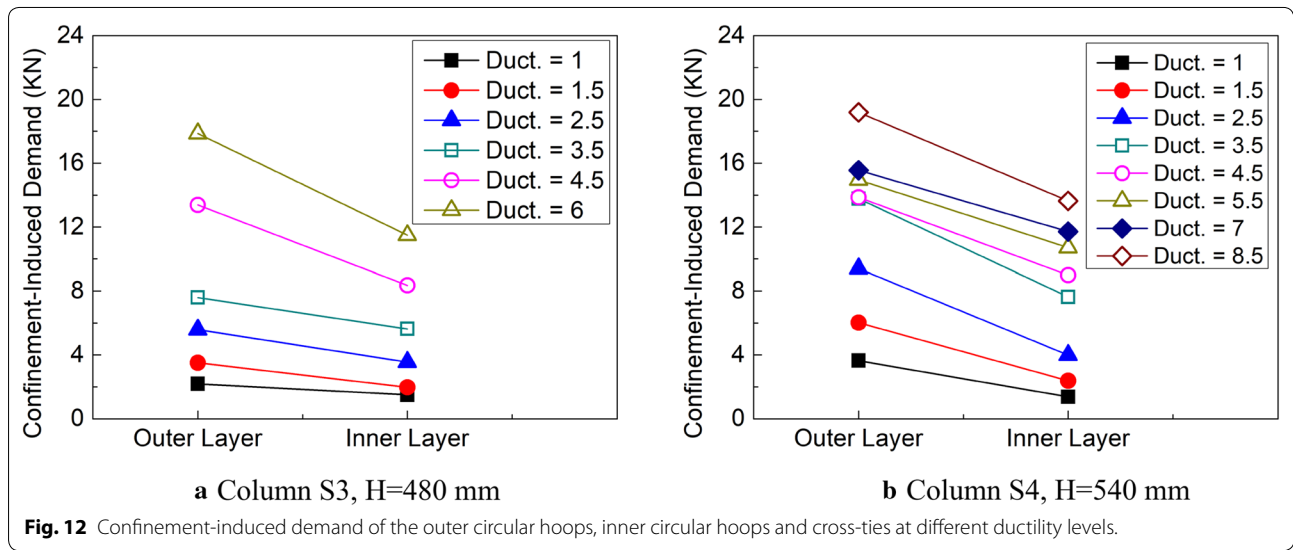
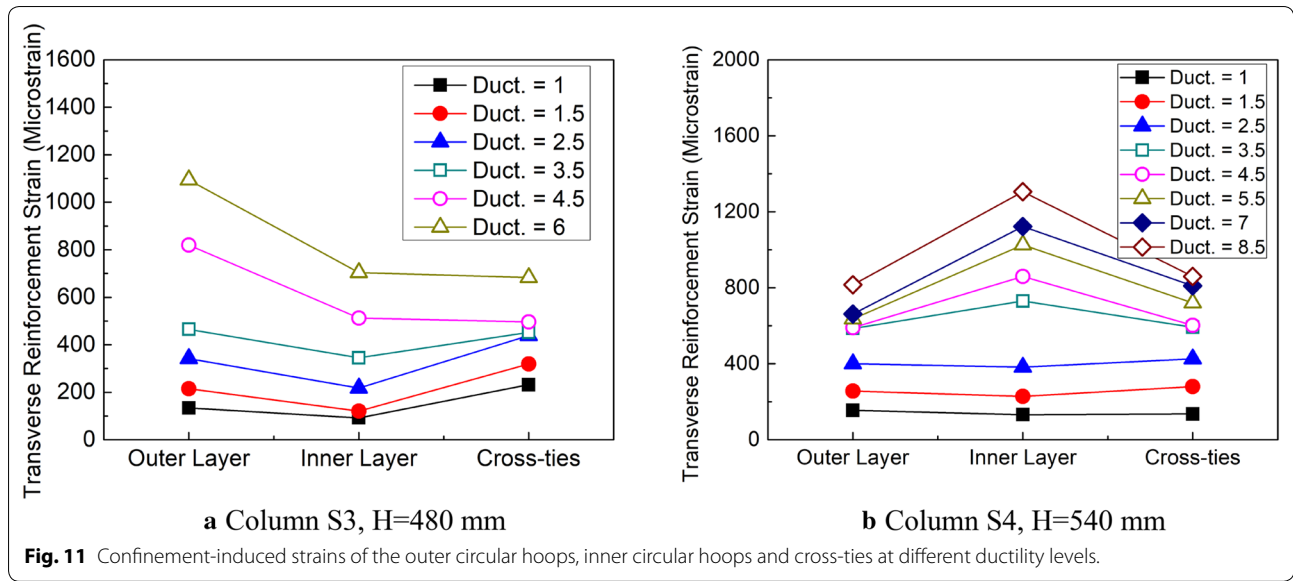
The confinement-induced strains of the outer circular hoops, inner circular hoops and cross-ties at the column height of 480 and 540 mm for columns S3 and S4 are shown in Fig. 11. It is found that the confinement-induced strains of the outer circular hoops, inner circular hoops and cross-ties increase with each increase of the ductility level. For column S3 with the same size of the outer circular hoops, inner circular hoops and cross-ties, the strains developed on the inner circular hoops are smaller than that at the outer circular hoops as shown in Fig. 11a. Different from column S3, the column S4 were reinforced with unequal sizes of the inner and outer circular hoops that have the same longitudinal spacing, and the strains developed on the inner circular hoops are greater than that on the outer circular hoops as shown in Fig. 11b. This is due to the smaller size of inner circular hoops used in column S4. If plotting the tension force (i.e., demand) developed on the outer circular hoops and inner circular hoops for



columns S3 and S4, the confinement-induced demand developed on the inner circular hoops are smaller than the outer circular hoops for both columns S3 and S4, as shown in Fig. 12. Therefore, the measured test data verified that the demand developed on the inner circular hoops are smaller than the outer circular hoops for circular hollow piers, which indicated that using a smaller size of inner circular hoops than the outer circular hoops was reasonable and effective.

4 Analysis of Hollow Column Response

In this section, the radial and circumferential confining stresses were first developed based on a detailed theoretical analysis to determine the confining stress in circular hollow RC piers. After that, an analytical approach was proposed to account for the confining effect in circular hollow RC piers, and this modeling approach was verified through comparisons with experimental results.



4.1 Theoretical Analysis

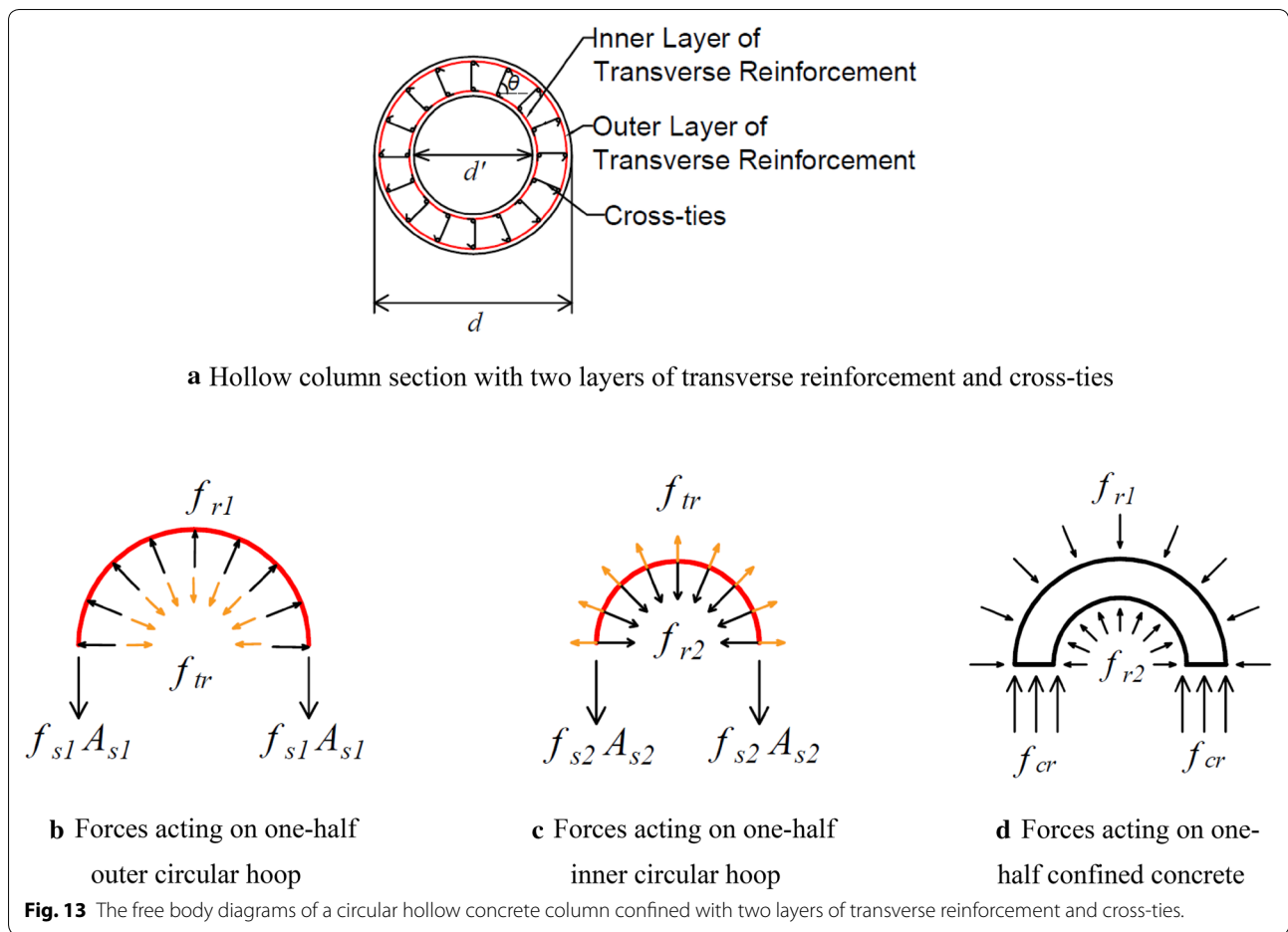
The confining effect of transverse reinforcement has been estimated based on the widely-used stress–strain response of the confined concrete model proposed by Mander et al. (1988). In this model, the confinement effect is represented by the confined strength ratio f'_{cc}/f'_c , where f'_{cc} is the compressive strength of confined concrete and f'_c is the compressive strength of unconfined concrete. The compressive strength of confined concrete f'_{cc} is defined as a function of effective confining stresses f'_l that is calculated based on the equilibrium equations. Similar to the confinement of concrete by circular hoops in solid concrete piers, the free body diagrams of a circular hollow concrete pier confined

with two layers of circular hoops and cross-ties when subjected to an axial compression load are shown in Fig. 13. Based on the forces developed in the cross-ties and inner circular hoop from the test data, it was found that

$$2f_{s2}A_{s2} < \sum F_{tr} \tag{2}$$

$$\sum F_{tr} = f_{tr}A_{tr} \cdot \sum \sin \theta \tag{3}$$

where $\sum F_{tr}$ is the resultant force of the confinement-induced force acting on cross-ties in one-half section, and θ is the angle between the cross-tie and the horizontal direction, as shown in Fig. 13a.



Therefore, the forces acting on one-half inner circular hoop is shown in Fig. 13c. Figure 13a presents the cross-section of a hollow concrete column confined with two layers of circular hoop and cross-ties, Fig. 13b shows the forces acting one-half outer circular hoop, Fig. 13c shows the forces acting on one-half inner circular hoop, and Fig. 13d shows the forces acting on one-half confined concrete.

Based on the free body diagrams of the outer circular hoop shown in Fig. 13b, equilibrium requires that

$$2f_{s1}A_{s1} + \sum F_{tr} = f_{r1} \cdot d \cdot s \tag{4}$$

Therefore,

$$f_{r1} = \frac{2f_{s1}A_{s1} + \sum F_{tr}}{d \cdot s} \tag{5}$$

Similarly, based on the free body diagrams of the inner circular hoop shown in Fig. 13c,

$$2f_{s2}A_{s2} + f_{r2} \cdot d' \cdot s = \sum F_{tr} \tag{6}$$

Therefore,

$$f_{r2} = \frac{\sum F_{tr} - 2f_{s2}A_{s2}}{d' \cdot s} \tag{7}$$

The free body diagram of the confined concrete is shown in Fig. 13d and the equilibrium requires that

$$f_{r1} \cdot d \cdot s = f_{r2} \cdot d' \cdot s + 2f_{cr} \cdot t \cdot s \tag{8}$$

Therefore,

$$\begin{aligned} f_{cr} &= \frac{f_{r1} \cdot d \cdot s - f_{r2} \cdot d' \cdot s}{2 \cdot t \cdot s} \\ &= \frac{2f_{s1}A_{s1} + \sum F_{tr} - \sum F_{tr} + 2f_{s2}A_{s2}}{2 \cdot t \cdot s} \\ &= \frac{f_{s1}A_{s1} + f_{s2}A_{s2}}{t \cdot s} \end{aligned} \tag{9}$$

From Fig. 13d, both the inside and outside concrete faces experience positive confining pressure. If the radial stress experienced by the hollow circular column was taken as the average of f_{r1} and f_{r2} , then

$$\begin{aligned}
 f_r &= \frac{f_{r1} \cdot d \cdot s + f_{r2} \cdot d' \cdot s}{2 \cdot \left(\frac{d+d'}{2}\right) \cdot s} \\
 &= \frac{2f_{s1}A_{s1} + \sum F_{tr} + \sum F_{tr} - 2f_{s2}A_{s2}}{(d + d') \cdot s} \quad (10) \\
 &= \frac{2(f_{s1}A_{s1} - f_{s2}A_{s2} + \sum F_{tr})}{(d + d') \cdot s}
 \end{aligned}$$

Based on the calculation shown above, the radial and circumferential confining stress experienced by the confined concrete in hollow piers with two layers of transverse reinforcement and cross-ties are expressed as Eqs. (11) and (12), respectively.

$$f_r = \frac{2(f_{s1}A_{s1} - f_{s2}A_{s2} + \sum F_{tr})}{(d + d') \cdot s} \quad (11)$$

$$f_{cr} = \frac{f_{s1}A_{s1} + f_{s2}A_{s2}}{t \cdot s} \quad (12)$$

As shown in Eqs. (11) and (12), the circular hollow column sections experience unequal magnitude of confining stresses in the radial and circumferential directions (i.e., $f_r \neq f_{cr}$), which is different from circular solid column sections. The confined concrete strength ratio f'_{cc}/f'_c was obtained based on the model proposed by Mander et al. (1988), which relates the compressive strength enhancement of confined sections to these two orthogonal confining stresses.

The radial confining stress f_r and circumferential confining stress f_{cr} experienced by the confined concrete in columns S3 and S4 at the maximum lateral displacement are shown in Table 4, using the measured strains of the outer circular hoop, inner circular hoop, and cross-ties at the column height of 480 and 540 mm, respectively. From this table, the confined strength ratio f'_{cc}/f'_c in column S4 is higher than that in column (i.e., 1.24 vs. 1.20), indicating better confinement effectiveness in column S4. This improved confined strength ratio in column S4 verifies that using smaller size of the inner circular hoops than the outer circular hoops helps to improve the confined concrete behavior in hollow piers.

It should be noted that the strains measured at the inner circular hoops, outer circular hoops, and cross-ties that were used to calculate the confined strength ratio (as shown in Fig. 11) were below the yield strains

at the column height of 480 and 540 mm. However, the confinement-induced strain profiles of the outer circular hoop indicated that the outer circular hoops reached the yield strain at the column height of 160 and 320 mm. Due to strain gauges were not placed on the inner circular hoops and cross-ties between the column height of 0 to 480/540 mm, strain data in these locations were not available. However, from the measured strains of the outer circular hoops, inner circular hoops and cross-ties at the column height of 480 and 540 mm as well as the finite element analyses by Liang and Sritharan (2018), the inner circular hoops and cross-ties would reach the yield strains after the outer circular hoops yielded. Therefore, the maximum developed confining stress in concrete occurs when the outer circular hoops, inner circular hoops and cross-ties reach their yield strengths. Referring to Eqs. (11) and (12), the maximum radial confining stress f_{r-max} and the maximum circumferential confining stress f_{cr-max} are:

$$f_{r-max} = \frac{2(f_{yh1}A_{s1} - f_{yh2}A_{s2} + \sum F_{tr})}{(d + d') \cdot s} \quad (13)$$

$$f_{cr-max} = \frac{f_{yh1}A_{s1} + f_{yh2}A_{s2}}{t \cdot s} \quad (14)$$

The maximum radial and circumferential confining stresses of columns S3 and S4 are listed in Table 5. For better comparison, the maximum radial and circumferential confining stresses experienced by the confined concrete in a solid column with the same dimension, the same reinforcement ratios and the same material properties are also included in Table 5. From this table, the compressive strength enhancement experienced by the confined concrete in hollow piers are higher than

Table 5 The maximum radial confining stress and the maximum circumferential confining stress experienced by the confined concrete in columns S3 and S4.

| Column | f_{r-max} (MPa) | f_{cr-max} (MPa) | f'_{cc}/f'_c |
|--------|-------------------|--------------------|----------------|
| S3 | 1.68 | 4.67 | 1.45 |
| S4 | 1.93 | 4.49 | 1.53 |
| Solid | 2.34 | 2.34 | 1.39 |

Table 4 The radial and circumferential confining stresses experienced by the confined concrete in columns S3 and S4.

| Column | f'_c (MPa) | f_r (MPa) | f_{cr} (MPa) | f_r/f'_c | f_{cr}/f'_c | f'_{cc}/f'_c |
|--------|--------------|-------------|----------------|------------|---------------|----------------|
| S3 | 33.8 | 0.6 | 1.83 | 0.0178 | 0.054 | 1.20 |
| S4 | 31.6 | 0.64 | 1.83 | 0.02 | 0.058 | 1.24 |

those in solid ones. It should be noted that the compressive strength enhancement of confined hollow section was related to the radial and circumferential confining stresses based on the model proposed by Mander et al. (1988). Although the circumferential confining stress of column S3 is somewhat higher, the reduction of radial confining stress of column S3 was more severe, when compared to column S4. Therefore, the resultant confined strength ratio f'_{cc}/f'_c of column S3 is smaller than column S4 (i.e., 1.45 vs. 1.53), indicating better confinement effectiveness for column S4.

4.2 Comparison of Experimental Responses with Analytical Response

To validate the proposed modeling method as described in the Sect. 4.1, pushover analyses of the test columns were carried out using the OpenSees.

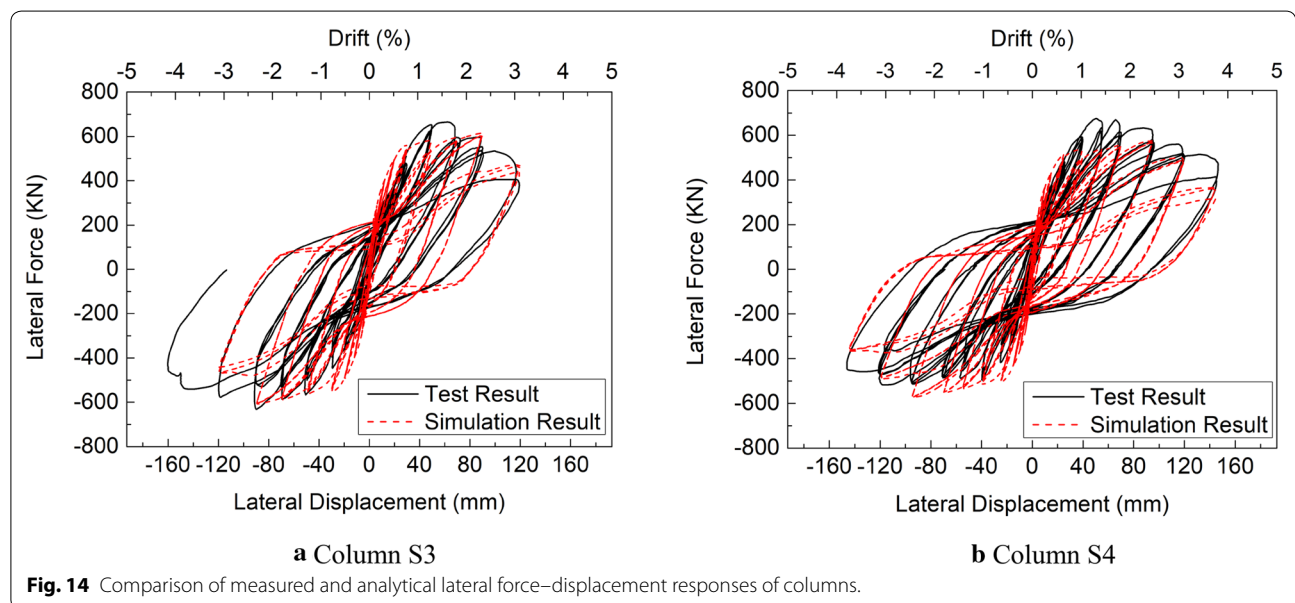
A two-dimensional *force beam column* element was used to simulate the flexural behavior of columns. The column cross-sections were approximately divided into longitudinal fiber cells and concrete fiber cells. These fiber cells were assigned uniaxial constitutive models with nonlinear material properties. The OpenSees *reinforcing steel* uniaxial material model with compression buckling, low-cycle fatigue and fracture of the bars was used to simulate the longitudinal reinforcing bars. The OpenSees *concrete07* material model was adopted to simulate the concrete. For the core concrete, the confinement effect in hollow piers was accounted by replacing the peak compressive strength and the corresponding strain with f'_{cc} and ϵ_{cc} , respectively. The values of f'_{cc} and ϵ_{cc} were defined by the confined concrete model proposed by Mander

et al. (1988), and the two orthogonal confining stresses were calculated based on the detailed theoretical analysis presented in the previous section. Besides the *force beam column* element, a *zero length section* element was constructed at the base of the column to simulate the bond slip of longitudinal reinforcing bars. The OpenSees *bond sp01* uniaxial material model (Zhao and Sritharan 2007) for capturing strain penetration effect at the column-to-footing intersections was assigned to the longitudinal reinforcement fiber cells instead.

Figure 14 shows the comparison between the measured lateral force–displacement responses and the analytical responses for columns S3 and S4. From this figure, the measured responses of the columns show a satisfactory agreement with the analytical responses, indicating that the analytical approach used to establish the stress–strain relationship of confined concrete in hollow piers could predict the flexure behavior of circular hollow RC piers.

5 Conclusions

The flexure behavior of two circular hollow RC piers with different amounts of the inner and outer circular hoops was investigated in this study. The confinement-induced transverse strains of the inner and outer circular hoops, as well as cross-ties within the plastic hinge regions, were recorded, and the confining stress in these hollow piers was developed based on a detailed theoretical analysis. According to the experimental and analytical results presented in this study, the following conclusions can be drawn:



- Both columns presented satisfactory hysteretic responses. Compared to column S3, column S4 showed more stable response under cycles of load reversals with a lower amount of confined concrete crushing (70 mm vs. 100 mm concrete wall thickness lost) and a higher level of ductility (7.8 vs. 6.7);
- The measured confinement-induced transverse strains of the outer circular hoops, inner circular hoops and cross-ties increase with each increase of ductility level;
- The measured confinement-induced transverse strains verify that the demand developed on the inner circular hoops are smaller than the outer circular hoops;
- The compressive strength enhancement experienced by the confined concrete in hollow piers are higher than those in solid ones. Also, compared to column S3 with the same size of inner and outer circular hoops, the column S4 with the smaller size of inner circular hoops than outer circular hoops experiences the higher value of confined strength ratio, indicating better confinement effectiveness; and
- The analytical approach used to establish the stress–strain relationship of confined concrete could predict the flexure behavior of circular hollow RC piers.

List of Symbols

B : the least dimension of the cross-section for columns; d_i : diameters of longitudinal reinforcing bar; ρ_l : the longitudinal reinforcement ratio; d_t : diameters of transverse reinforcement; ρ_t : transverse volumetric reinforcement ratio; μ_s : displacement ductility; Δ_u : the displacement at ultimate; Δ_y : the displacement at yield; A_{s1} : cross-sectional area of the outer circular hoop; A_{s2} : cross-sectional area of the inner circular hoop; A_{tr} : cross-sectional area of cross-ties; A_g : gross area of a concrete section; A_c : cross-sectional area of a structural member measured to the outside edges of transverse reinforcement; ΣF_{tr} : the resultant force of the confinement-induced force acting on cross-ties in one-half section; θ : the angle between the cross-tie and the horizontal direction; f_{s1} : confinement-induced steel stress of outer circular hoop; f_{s2} : confinement-induced steel stress of inner circular hoop; f_{tr} : confinement-induced steel stress of cross-ties; f_{r1} : radial confining stress induced by outer circular hoop; f_{r2} : radial confining stress induced by inner circular hoop; f_{cr} : circumferential confining stress; f_c : concrete compressive stress; f_{cc}' : compressive strength of confined concrete; f_{r-max} : maximum radial confining stress; f_{cr-max} : maximum circumferential confining stress; f_e' : effective confining stresses; f_{yh1} : the yield strength of outer transverse reinforcement; f_{yh2} : the yield strength of inner transverse reinforcement; f_{yt} : the yield strength of cross-ties; P : column axial load; d : core diameter of circular hollow column embraced by the transverse reinforcement; d' : inner diameter of the circular hollow column; t : wall thickness of the circular hollow column; s : center-to-center spacing of confinement reinforcement.

Acknowledgements

This research is funded by the National Natural Science Foundation of China under grant Nos. 51427901 and 51808380 as well as Tianjin Municipal Science and Technology Commission under grant No. 17JCYBJC42500. Their supports are gratefully acknowledged.

Authors' contributions

ZXL supervised this project and discussed the overall research such as the test plan, test results, and conclusions. He also suggested the test variables and the main structure of this paper. BZ designed the testing program. CD and XL carried out the experiments, analyzed the data, and wrote the paper. All authors read and approved the final manuscript.

Funding

This research is funded by the National Natural Science Foundation of China under Grant Nos. 51427901 and 51808380 as well as Tianjin Municipal Science and Technology Commission under Grant No. 17JCYBJC42500.

Availability of data and materials

Not applicable.

Competing interests

The authors declare that they have no competing interests.

Author details

¹ Key Laboratory of Coast Civil Structure Safety of Ministry of Education, Tianjin University, Tianjin 300350, China. ² Tianjin Key Laboratory of Civil Structure Protection and Reinforcement, Tianjin Chengjian University, Tianjin 300384, China.

Received: 1 August 2019 Accepted: 6 December 2019

Published online: 10 February 2020

References

- Caltrans Seismic Design Criteria (2017) California Department of Transportation Sacramento, CA.
- Calvi, G. M., Pavese, A., Rasulo, A., & Bolognini, D. (2005). Experimental and numerical studies on the seismic response of R.C. hollow bridge piers. *Bulletin Earthquake Engineering*, 3(3), 267–297.
- Cascard, A., Micelli, F., & Aiello, M. A. (2016). Unified model for hollow columns externally confined by FRP. *Engineering Structures*, 111, 119–130.
- Guidelines for Seismic Design of Highway Bridges (JTG/T B02-01—2008) (2008) Ministry of Transport of the People's Republic of China.
- Han, Q., Du, X. L., Zhou, Y. H., & Lee, G. C. (2013). Experimental study of hollow rectangular bridge column performance under vertical and cyclically bilateral loads. *Earthquake Engineering and Engineering Vibration*, 12(3), 433–445.
- Hwang, S. K., & Yun, H. D. (2004). Effects of transverse reinforcement on flexural behavior of high-strength concrete columns. *Engineering Structures*, 26(1), 1–12.
- Lee, J. H., Choi, J. H., Hwang, D. K., & Kwahk, I. J. (2015). Seismic performance of circular hollow RC bridge columns. *Journal of Civil Engineering, KSCE*, 19(5), 1456–1467.
- Liang, X., & Sritharan, S. (2018). Effects of confinement in circular hollow concrete columns. *Journal of Structural Engineering, ASCE*, 144(9), 04018159.
- Liao, W. C., Perceka, W., & Wang, M. (2017). Experimental study of cyclic behavior of high-strength reinforced concrete columns with different transverse reinforcement detailing configurations. *Engineering Structures*, 153, 290–301.
- Mander, J. B., Priestley, M. J. N., & Park, R. (1988). Theoretical stress-strain model for confined concrete. *Journal of Structural Engineering, ASCE*, 144(8), 1804–1826.
- Mo, Y. L., Wong, D. C., & Maekawa, K. (2003). Seismic performance of hollow bridge columns. *ACI Structural Journal*, 100(3), 337–348.
- Moehle, J. P., & Bavanagh, T. (1985). Confinement effectiveness of crossties in RC. *Journal of Structural Engineering*, 111(10), 2105–2120.
- Papanikolaou, V. K., & Kappos, A. J. (2009a). Numerical study of confinement effectiveness in solid and hollow reinforced concrete bridge piers: Methodology. *Computers & Structures*, 87(21–22), 1427–1439.
- Papanikolaou, V. K., & Kappos, A. J. (2009b). Numerical Study of confinement effectiveness in solid and hollow reinforced concrete bridge piers: Analysis results and discussion. *Computers & Structures*, 87(21–22), 1440–1450.
- Penelis, G. G., & Kappos, A. J. (1997). *Earthquake-resistant concrete structures*. London and New York: Taylor & Francis.

- Pinto, A. V., Molina, J., & Tsionis, G. (2003). Cyclic tests on large-scale models of existing bridge piers with rectangular hollow cross-section. *Earthquake Engineering and Structural Dynamics*, 32(13), 1995–2012.
- Prado, N. I., Aguilar, G., López, O., Gómez, R., & Escobar, J. A. (2016). Arrangement of transverse reinforcement in hollow piers subjected to lateral load. *ACI Structural Journal*, 113(4), 723–733.
- Priestley, M. J. N., Seible, F., & Calvi, G. M. (1996). *Seismic design and retrofit of bridges*. New York: Wiley.
- Rousakis, T. C., Karabinis, A. I., & Kioussis, P. D. (2007). FRP-confined concrete members: Axial compression experiments and plasticity modeling. *Engineering Structures*, 29(7), 1343–1353.
- Yeh, Y. K., Mo, Y. L., & Yang, C. Y. (2001). Seismic performance of hollow circular bridge piers. *ACI Structural Journal*, 98(6), 862–871.
- Yeh, Y. K., Mo, Y. L., & Yang, C. Y. (2002). Full-scale tests on rectangular hollow bridge piers. *Materials and Structures*, 35(2), 117–125.
- Zhao, J., & Sritharan, S. (2007). Modeling of strain penetration effects in fiber-based analysis of reinforced concrete structures. *ACI Structural Journal*, 104(2), 133–141.

Publisher's Note

Springer Nature remains neutral with regard to jurisdictional claims in published maps and institutional affiliations.

Submit your manuscript to a SpringerOpen[®] journal and benefit from:

- ▶ Convenient online submission
- ▶ Rigorous peer review
- ▶ Open access: articles freely available online
- ▶ High visibility within the field
- ▶ Retaining the copyright to your article

Submit your next manuscript at ▶ [springeropen.com](https://www.springeropen.com)
